Iraqi Journal of Science, 2020, Vol. 61, No. 10, pp: 2570-2581
DOI: 10.24996/ijs.2020.61.10.13

ISSN: 0067-2904

Zeta Potential of Ag, Cu, ZnO, CdO and Sn Nanoparticles Prepared by Pulse Laser Ablation in Liquid Environment

Dalya K. Naser*[1], Ahmed K. Abbas[1], Kadhim A. Aadim[2]
[1]Department of Physics, College of Science , University of Wasit, Wast, Iraq
[2]Department of Physics, College of Science, University of Baghdad, Baghdad, Iraq

Received: 14/10/2019 Accepted: 17/12/2019

Abstract:
Metal nanoparticles (NPs) of silver (Ag), copper (Cu), zinc oxide (ZnO), cadmium oxide (CdO) and tin (Sn) were synthesized by laser ablation of a solid target in de-ionized water (DI). X-ray diffraction patterns showed the formation of AgO, Ag, Cu, ZnO, CdO, and Sn NPs. Absorbance spectrum of the produced nanoparticles was measured by UV-Vis spectrophotometer which showed that Ag and CdO NPs shifted to the short wavelength (blue shift), indicating the formation of NPs with smaller sizes, whereas CuO showed the formation two peaks. ZnO and Sn NPs shifted to the long wavelength (red shift) which indicates the formation NPs with larger size. Zeta potential results proved that ZnO nanoparticles were more stable (-26.53mV) than the other metal nanoparticles, while CdO nanoparticles had more aggregation (-16.65mV).

Keywords: metal nanoparticles (NMNPs), pulse laser ablation, zeta potential.

زيتا للجسيمات الفضة, النحاس, اوكسيد الزنك, اوكسيد الكادميوم والقصدير النانوية المحضرة بواسطة استئصال الليزر النبضي في البيئة السائلة

داليا خالد*[1]، احمد خضير[1]، كاظم عبد الواحد[2]
[1]قسم الفيزياء، كلية العلوم، جامعة واسط، واسط ، العراق
[2]قسم الفيزياء، كلية العلوم، جامعة بغداد، بغداد، العراق

الخلاصة
تم تصنيع جسيمات النانوية المعدنية (الفضة, النحاس ,اوكسيد الزنك, اوكسيد الكادميوم, القصدير) بواسطة الاستئصال بالليزر النبضي لهدف صلب في ماء منزوع الايونات. اظهر نمط حيود الاشعة السينية تشكيل جسيمات نانوية للفضة, اوكسيد الفضة, النحاس, اوكسيد الزنك, اوكسيد الكادميوم والقصدير. تم قياس طيف الامتصاصية لمحاليل الجسيمات النانوية الناتجة بواسطة مقاس الطيف الضوئي للأشعة الفوق بنفسجية والذي يوضح ان جسيمات الفضة واكسيد الكادميوم النانوي يتجه نحو الاطوال الموجية القصيرة(الزرقاء) والتي تشير الى تكوين جسيمات نانوية بأحجام صغيرة, جسيمات النحاس النانوية تكون قمتين. بينما جسيمات اوكسيد الزنك والقصدير النانوية تتزحف نحو الاطوال الموجية الاطول (الحمراء) وهذا يشير الى تكوين جسيمات نانوية بأحجام اكبر. اثبتت نتائج احتمالية زيتا ان جسيمات اوكسيد الزنك النانوية هي الاكثر استقرارا(−26,53ملي فولت) من الجسيمات النانوية الاخرى, في حين ان جسيمات اوكسيد الكادميوم هي الاكثر تجميع(−16,65ملي فولت) من الجسيمات النانوية المعدنية الاخرى.

*Email: Daliya.khaled92@gmail.com

Introduction

Nanotechnology demands the ability to control features at the nanoscale (10^{-9} m) [1]. Nanoparticles are the fundamental structures in nanotechnology, which has many applications in different areas such as biosensor and electronic nanodevices [2, 3]. Nanoparticles' properties show large differences in electrical, optical, magnetic and chemical properties from the bulk material they are made from [4], because they have large surface area to volume ratio as compared to bulk, quantum confinement, and Plasmon excitation [5]. Nano-sized metals with a size range of 10-100nm are metallic nanoparticles. Metallic nanoparticles have unique features such as surface resonance of Plasmon (SPR) and optical properties [6]. The bright colors of noble metal nanoparticles are due to the resonant excitation of a collective oscillation of the conduction band electrons in the particles, termed the particle Plasmon. The SPR absorption of those metal NPs is dependent on their size, shape and composition [7]. Laser ablation in liquid environment (PLAL) is a "top-down" nanoparticles processing method and has many advantages over chemical techniques; it does not require expensive vacuum chambers and sophisticated equipment, while it is also a simple and clean method where it is possible to control poor agglomeration, size, and shape of NPs by optimizing some experimental parameters [8-13].

Zeta potential (ZP), also known as electrokinetic potential, is a stability measure of the load and governs all interactions between particles in a suspension [14]. ZP has values between + 100 mV and -100 mV. It is well known that higher absolute values of zeta potential mean higher stable status of colloidal systems, while potential values higher than + 30 mV or lower than -30 mV allow for significantly stable suspension [15,16] . ZP depends on a number of factors, such as the velocity of the moving particle under the influence of the electrical field and the dispersion media viscosity [17].

In the present work, pulse laser ablation in deionized water was prepared for Ag, Cu, Zn, Sn, and Cd and their characterization was studied.

Experimental Part

Metal nanoparticles (MNPs) and metal oxide nanoparticles were produced by laser ablation at room temperature of high-purity targets of Ag, Cu, Zn, Cd, and Sn. Figure-1 demonstrates the schematic representation of the pulsed-laser ablation in liquid (PLAL) system. The laser beam was focused by a lens with a focal length 10 cm. Subsequently, metal targets were placed at the bottom of a quartz vessel filled with 3 ml of liquid and irradiated with Q-switched Nd:YAG laser operated with emission wavelength at 1064 nm, with pulse duration of 10 ns and a repeat frequency of 6 Hz. The laser energies were used with 100-500mJ to ablate metal targets. Thin film was obtained with a drop-casting technique of 500mJ and 500 pulses to instill the collide fluid on a glass substratum in order to obtain a uniform distributed thin film of nanoparticles. The crystalline structure was studied using X-ray diffractometer (Philips PW). A spectrometer (type SP-8001-Metertech) reported the UV-Vis absorption spectra of noble metal colloids. The zeta potential calculation was conducted using a Zeta Plus (Brookhaven Instruments Corporation, USA).

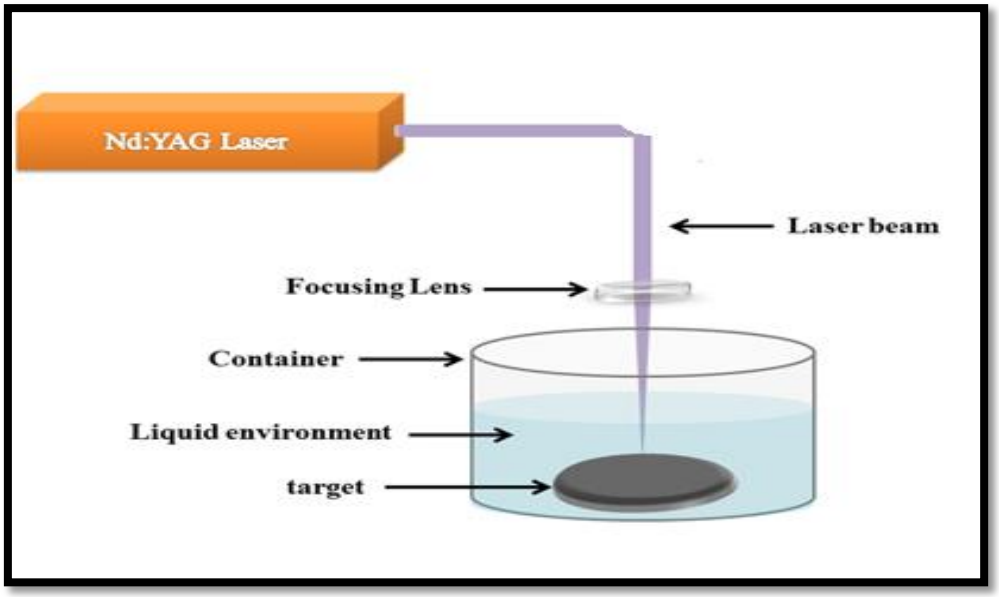

Figure 1-Schematic diagram of PLAL system.

Results and Discussion

1-The structural analysis

Figure-2 shows the formation of AgO and Ag NPs prepared by PLAL of an Ag target which has a polycrystalline structure of monoclinic and cubic phases. There is a matching between the orientation of the Miller Indices (hkl) to each peak for Ag NPs with the JCPDS standard card of these planes, i.e. (11-1), (111), and (202) planes . Figure-3 shows that Cu NPs have a polycrystalline structure and a cubic phase, while there was a matching between the orientation of the Miller Indices (hkl) to each peak for Cu NPs with (111) and (200) planes. Figure-4 shows that the formation ZnO NPs has a polycrystalline structure and hexagonal phase for ZnO NPs. The peaks were at (100), (002), and (101) planes. Figure-5 shows that the formation CdO NPs has a polycrystalline structure and a cubic phase, with peaks at (111) and (200) planes. Figure-6 shows that Sn NPs have a polycrystalline structure and a tetragonal phase with peaks at (200), (101), (220), and (211) planes. As shown in Tables-1 to 5, the increase in the sharpness of XRD peaks indicates that the particles are in a crystalline nature of metal nanoparticles (Ag, Cu, ZnO, CdO and Sn, respectively).

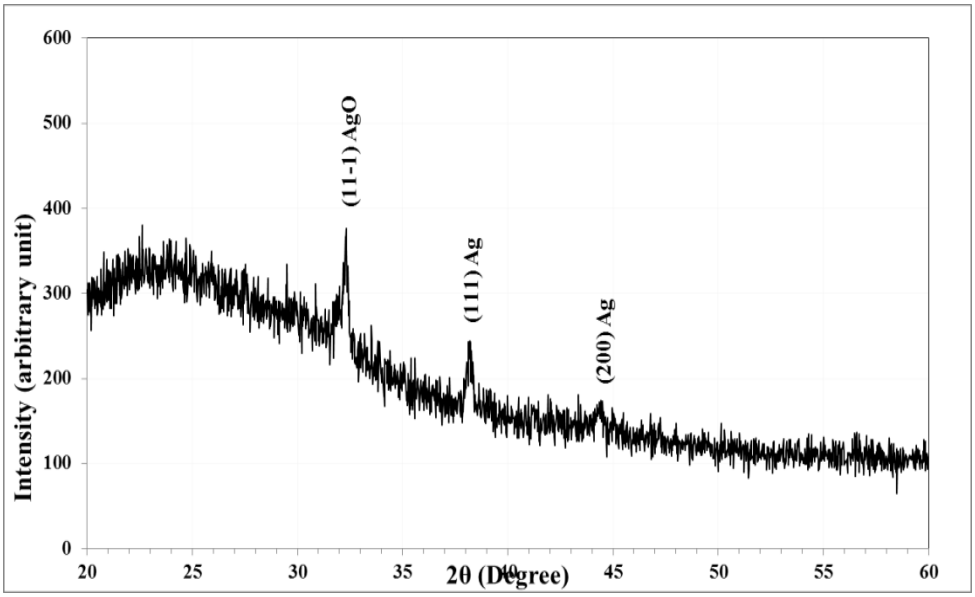

Figure 2-XRD spectrum of experimental pattern of Ag NPs.

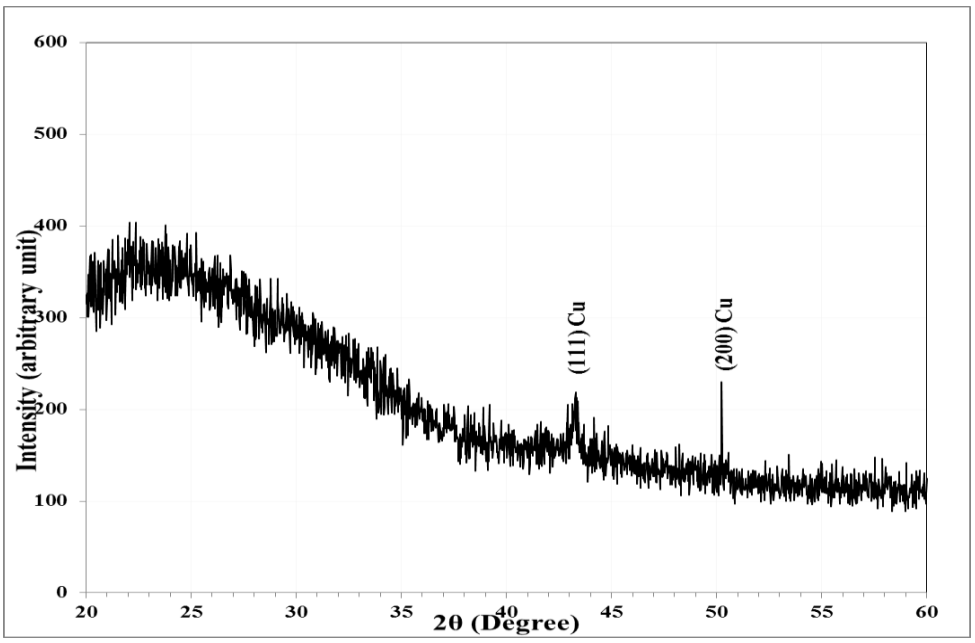

Figure 3-XRD spectrum of experimental pattern of Cu NPs.

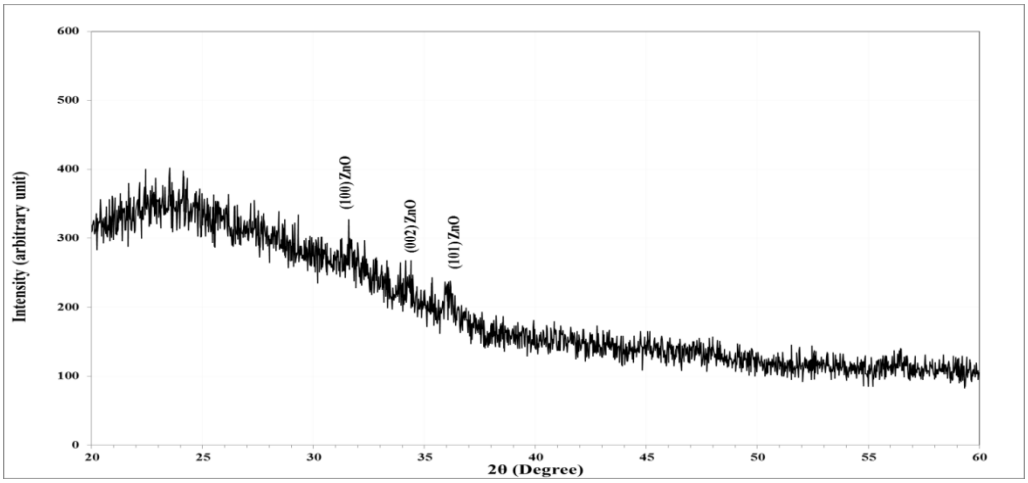

Figure 4-XRD spectrum of experimental pattern of ZnO NPs.

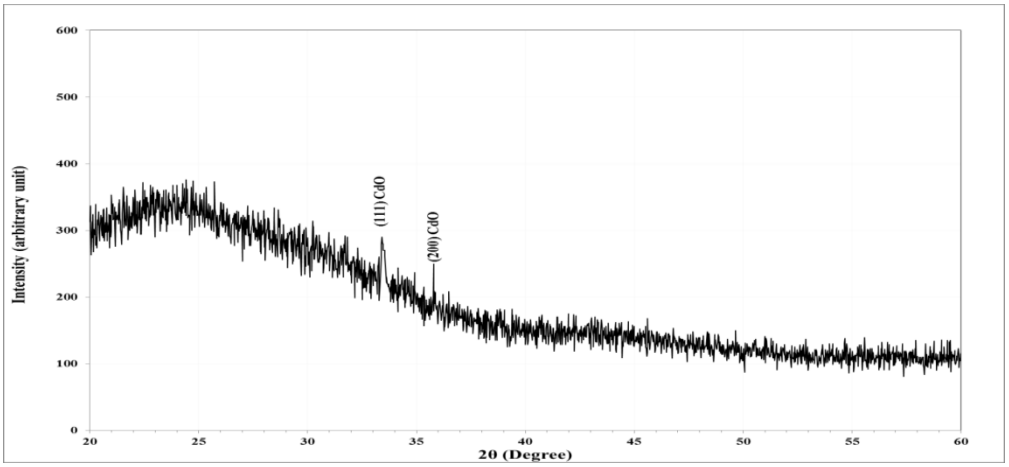

Figure 5-XRD spectrum of experimental pattern of CdO NPs.

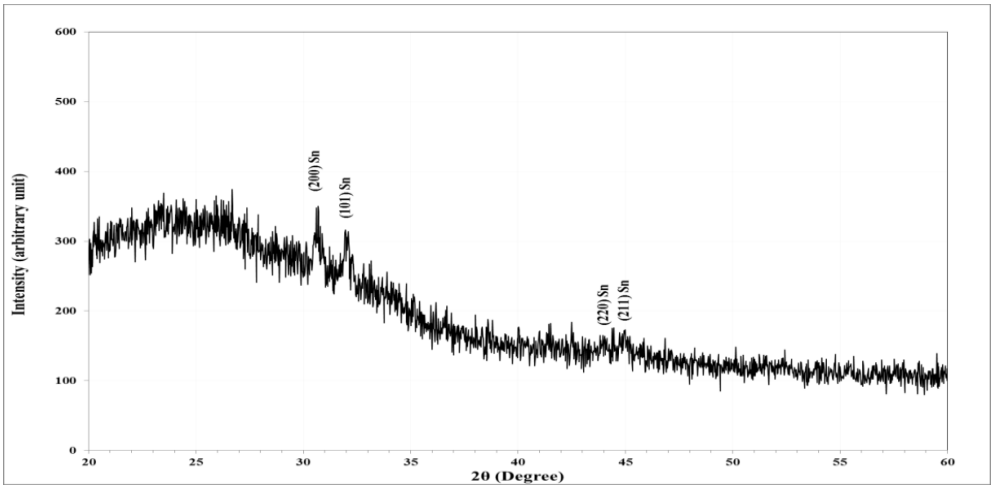

Figure 6-XRD spectrum of experimental pattern of Sn NPs.

Table 1-The structural parameters viz. inter-planar spacing and crystallite size (D) of Ag NPs

2θ (Deg.)	FWHM (Deg.)	d_{hkl} Exp.(Å)	C.S (nm)	d_{hkl} Std.(Å)	hkl	Phase	card No.
32.3517	0.4908	2.7650	16.9	2.7669	(11-1)	Mono.AgO	96-900-8963
38.1595	0.4090	2.3565	20.6	2.3592	(111)	Cub. Ag	96-900-8460
44.4581	0.4908	2.0362	17.5	2.0431	(200)	Cub. Ag	96-900-8460

Table 2-The structural parameters viz. inter-planar spacing and crystallite size (D) of Cu NPs

2θ (Deg.)	FWHM (Deg.)	d_{hkl} Exp.(Å)	C.S (nm)	d_{hkl} Std.(Å)	hkl	Phase	card No.
43.3094	0.5344	2.0875	16.0	2.0958	(111)	Cub. Cu	96-901-3016
50.2569	0.6577	1.8140	13.3	1.8150	(200)	Cub.Cu	96-901-3016

Table 3-The structural parameters viz. inter-planar spacing and crystallite size (D) of ZnO NPs

2θ (Deg.)	FWHM (Deg.)	d_{hkl} Exp.(Å)	C.S (nm)	d_{hkl} Std.(Å)	hkl	Phase	card No.
31.6116	0.3306	2.8281	25.0	2.8174	(100)	Hex.ZnO	96-900-4182
34.2975	0.4958	2.6125	16.8	2.6037	(002)	Hex.ZnO	96-900-4182
36.1157	0.5785	2.4850	14.4	2.4780	(101)	Hex.ZnO	96-900-4182

Table 4-The structural parameters viz. inter-planar spacing and crystallite size (D) of CdO NPs

2θ (Deg.)	FWHM (Deg.)	d_{hkl} Exp.(Å)	C.S (nm)	d_{hkl} Std.(Å)	hkl	Phase	card No.
33.4298	0.3306	2.6783	25.1	2.6811	(111)	Cub. CdO	96-900-6691
35.7851	0.2892	2.5072	28.9	3.3219	(200)	Cub. CdO	96-900-6691

Table 5-The structural parameters viz, inter-planar spacing and crystallite size (D) of Sn NPs

2θ (Deg.)	FWHM (Deg.)	d_{hkl} Exp.(Å)	C.S (nm)	d_{hkl} Std.(Å)	hkl	Phase	card No.
30.6528	0.4560	2.9143	18.1	2.9098	(200)	Tet. Sn	96-900-8571
32.0207	0.4559	2.7929	18.1	2.7871	(101)	Tet. Sn	96-900-8571
43.9171	0.4560	2.0600	18.8	2.0576	(220)	Tet. Sn	96-900-8571
44.9534	0.5389	2.0149	16.0	2.0128	(211)	Tet. Sn	96-900-8571

2-Absorption spectra of Ag, Cu, Zn, Cd and Sn NPs

The solution prepared in this study for the metals' nanoparticles has a Plasmon peak. Figures-(7-11) display the absorbance spectra of Ag, Cu, Zn, Cd and Sn NPs, which varied with different laser powers (100, 200,300,400 and 500 mJ, respectively) at 500 pulses. The absorbance indicated that the increased intensity lead to increased Plasmon peak with an increase in laser power, suggesting an increase in NP concentration [18]. The spectra show plasmon resonance peaks of Ag, Cu, ZnO, CdO and Sn due to quantum size effects at UV ranges of 403-406, 649-653, 304-319, 276-293 and 303-315 nm, respectively, as shown in tables (6) to (10). Tables-(6, 9) show the peak absorbance of Ag, AgO and CdO NPs at different laser powers; as the energy increased, the peak became narrower and shifted to the short wavelength (blue shift, which indicates the formation of Ag and CdO NPs with smaller sizes. Table-7 shows two absorbance peaks of Cu NPs at different laser powers; the first peak is stable at 297 nm and the second is a Plasmon peak that is shifted to the short wavelength (blue shift), indicating the formation of Cu NPs with smaller size. Tables-(8, 10) show the absorbance peaks of ZnO and Sn NPs at different laser powers , which are shifted to the large wavelength (red shift), indicating the formation of ZnO and Sn NPs with larger sizes as the power increases.

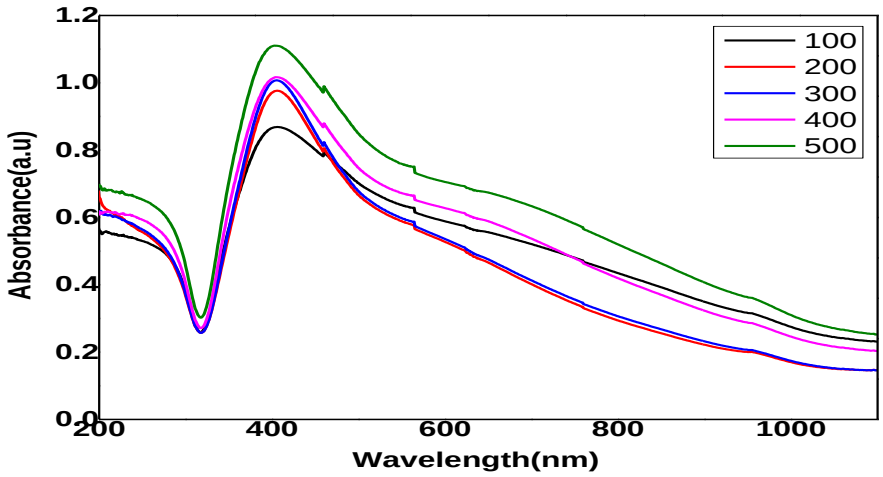

Figure 7-Optical Absorbance as a Function of Wavelength for Ag NPs Colloidal Solution.

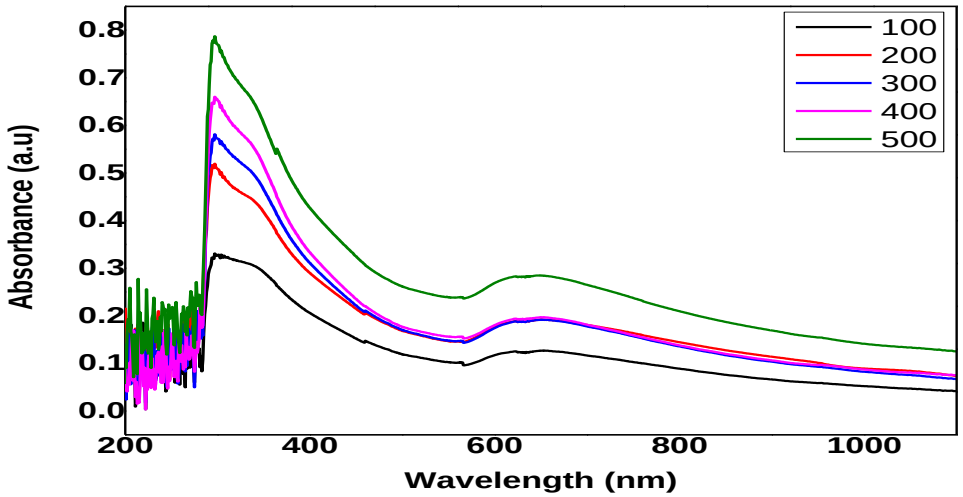

Figure 8-Optical Absorbance as a Function of Wavelength for Cu NPs Colloidal Solution.

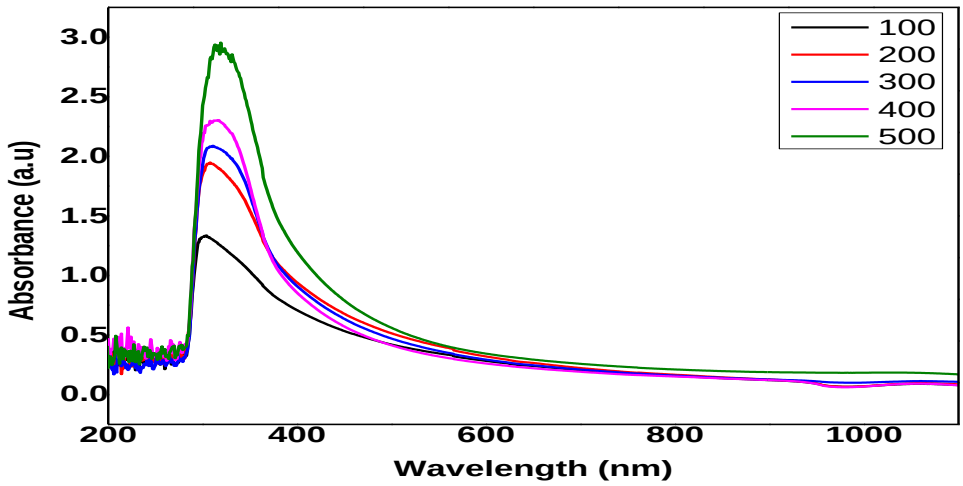

Figure 9-Optical Absorbance as a Function of Wavelength for Zn NPs Colloidal Solution.

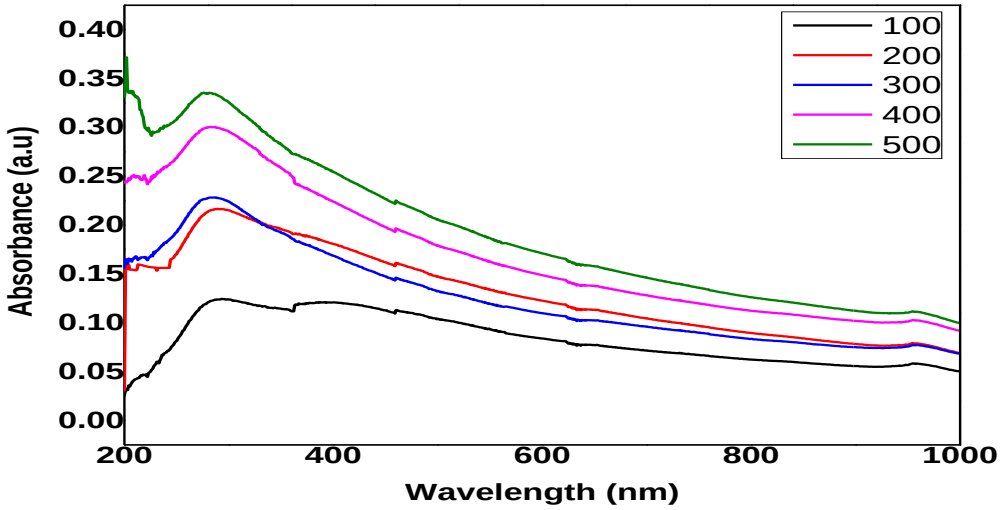

Figure 10-Optical Absorbance as a Function of Wavelength for Cd NPs Colloidal Solution.

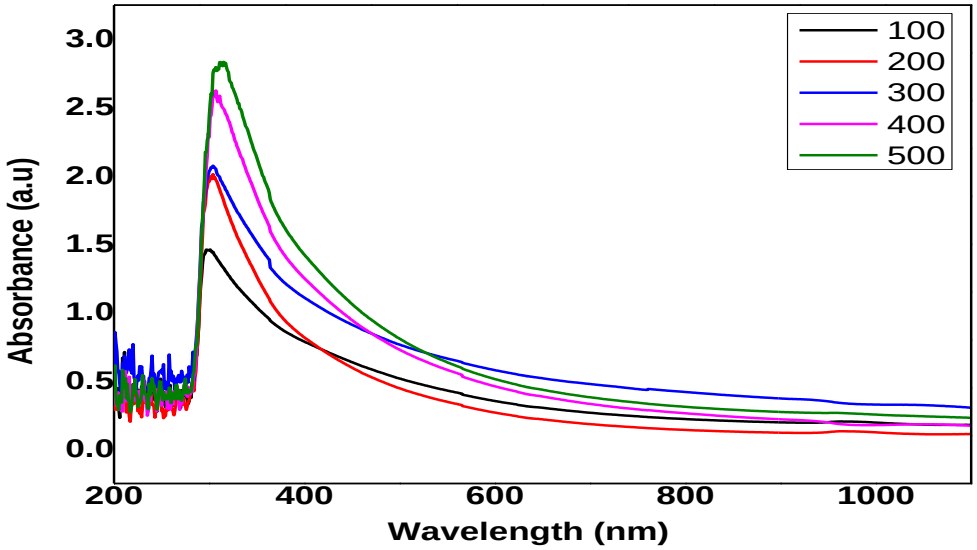

Figure 11-Optical Absorbance as a Function of Wavelength for Sn NPs Colloidal Solution.

Table 6-Peak Position and Absorbance of Ag NPs at Different Power and 500 Pulses

Metal Nanoparticle	Power(mJ)	Absorbance	Peak Position (nm)
Ag	100	0.8689	406
	200	0.9766	406
	300	1.0074	405
	400	1.017	404
	500	1.1106	403

Table 7-Peak Position and Absorbance of Cu NPs at Different Power and 500 Pulses

Metal Nanoparticle	Power(mJ)	Absorbance	Peak Position (nm)
Cu	100	0.1273	653
	200	0.1923	651
	300	0.1924	651
	400	0.1974	650
	500	0.2852	649

Table 8-Peak Position and Absorbance of ZnO NPs at Different Power and 500 Pulses

Metal Nanoparticle	Power(mJ)	Absorbance	Peak Position (nm)
Zn	100	1.3362	304
	200	1.9484	308
	300	2.0892	311
	400	2.3045	317
	500	2.9545	319

Table 9-Peak Position and Absorbance of CdO NPs at Different Power and 500 Pulses

Metal Nanoparticle	Power (mJ)	Absorbance	Plasmon Peak (nm)
CdO	100	0.1245	293
	200	0.2167	289
	300	0.2283	286
	400	0.3006	282
	500	0.3356	276

Table 10-Peak Position and Absorbance of Sn NPs at Different Power and 500 Pulses

Metal Nanoparticles	Power(mJ)	Absorbance	Peak Position (nm)
Sn	100	1.4618	301
	200	2.0748	304
	300	2.0134	304
	400	2.6249	307
	500	2.8339	315

3- Color Dependence of Nanoparticles

The synthesis of Ag, Cu, ZnO, CdO and Sn NPs using the pulse laser ablation on silver, ,copper, zinc, cadmium, and tin metal plates was confirmed by the color change. Figure-12 shows that the color of the solution was observed to change from clear to dark brown for Ag NPs, green for Cu NPs, light brown for ZnO and Sn NPs, and white with a high concentration for Cd NPs. The figure shows the change in color as a function of the concentration of nanoparticles by adjusting certain parameters as shown in each duct. The important optical is metal nanoparticles attributes, as distributed in their bright intense colors [19].

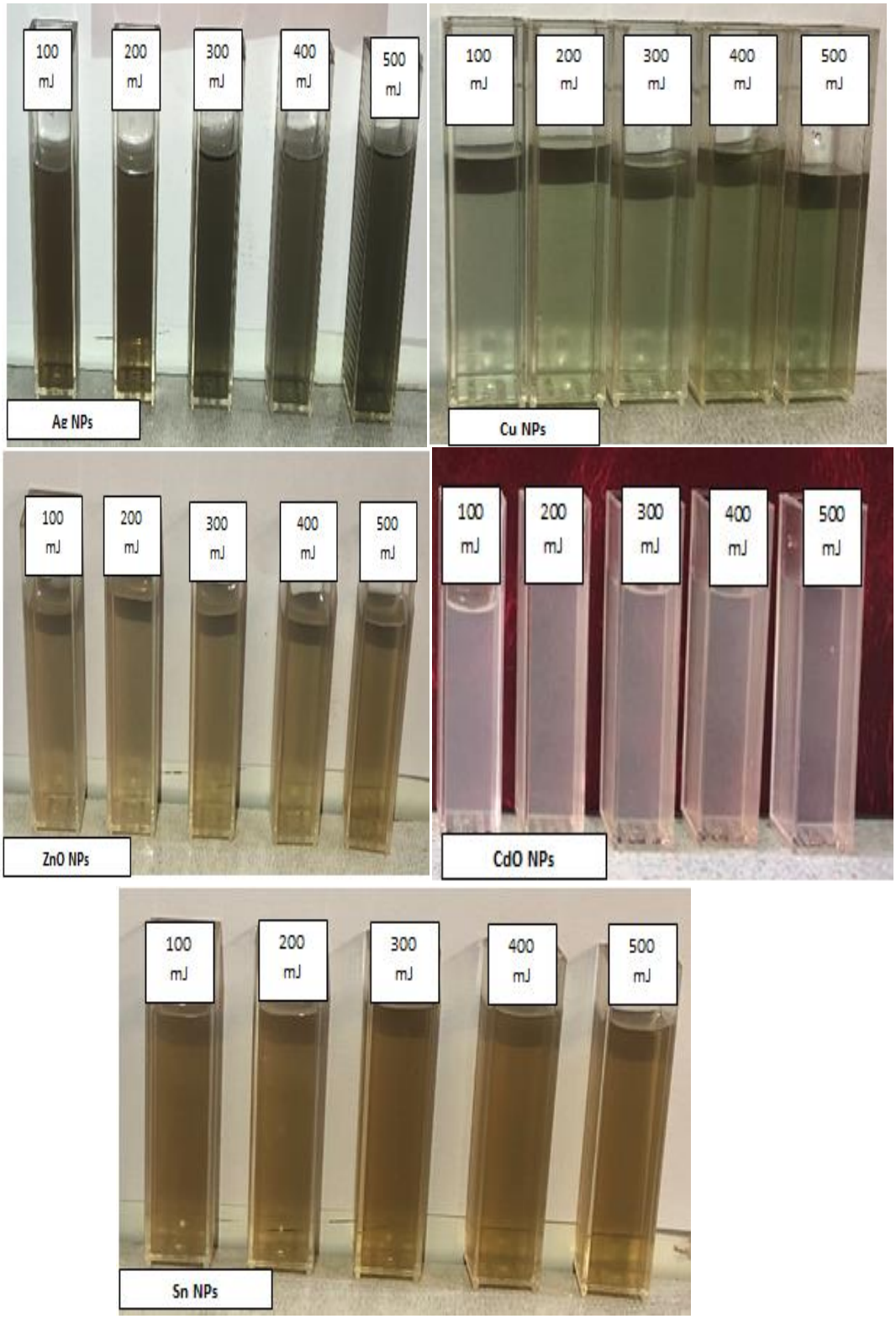

Figure 12-An image of the final products of metal NP solutions prepared by laser ablation.

4- Zeta Potential of Ag, Cu, ZnO, CdO and Sn NPs

ZP demonstrates the stability of colloidal nanoparticles. Figures- 13-17 display the zeta potential values of Ag, Cu, ZnO, CdO, and Sn NP at 500 mJ laser power and 500 pulses, which were, respectively, -23.67, -22.04, -26.53, -16.65 and -25.17mV. Notice that in the colloidal solution, more negative values indicate more stability of NPs.

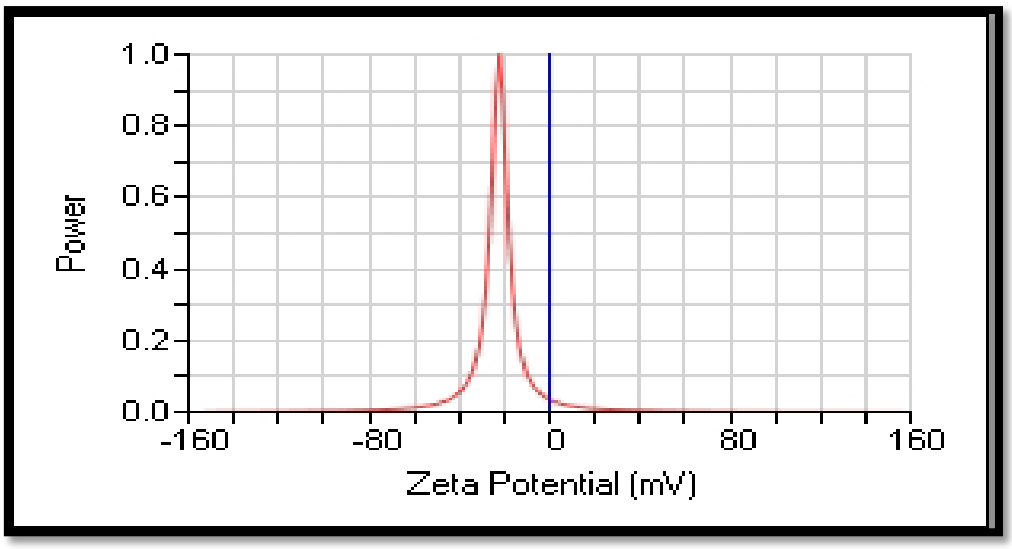

Figure 13-Zeta potential of Ag NPs

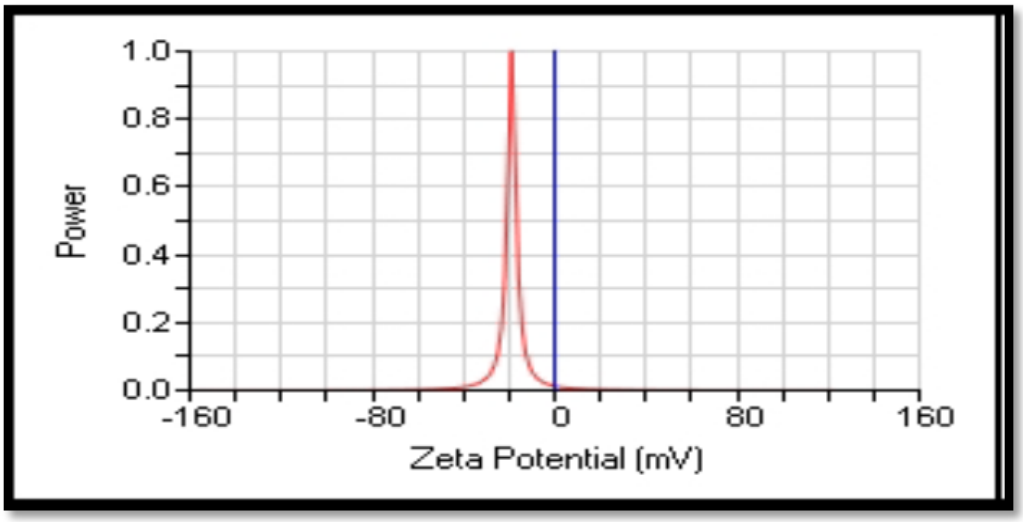

Figure 14-Zeta potential of Cu NPs.

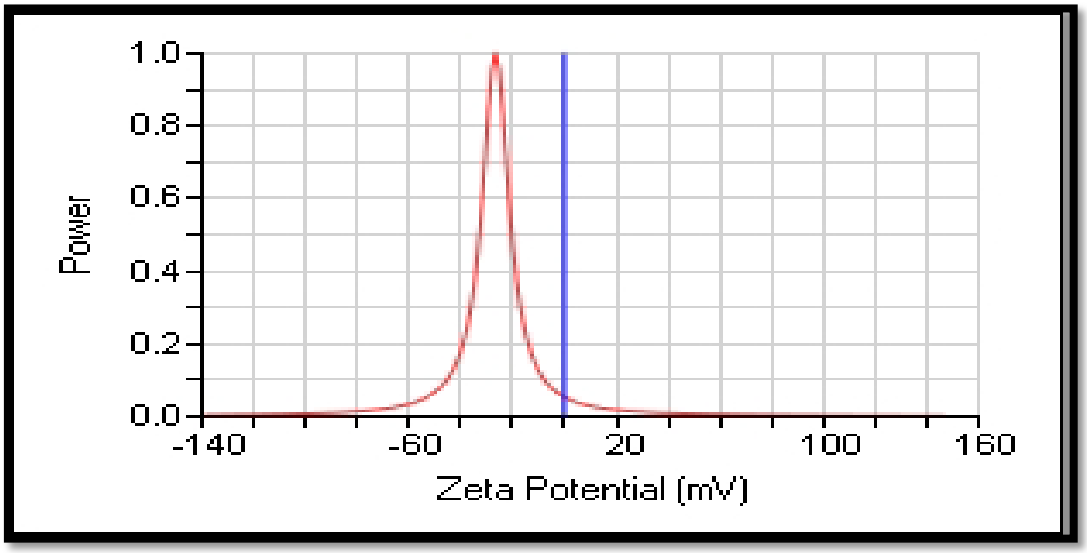

Figure 15- Zeta potential of ZnO NPs.

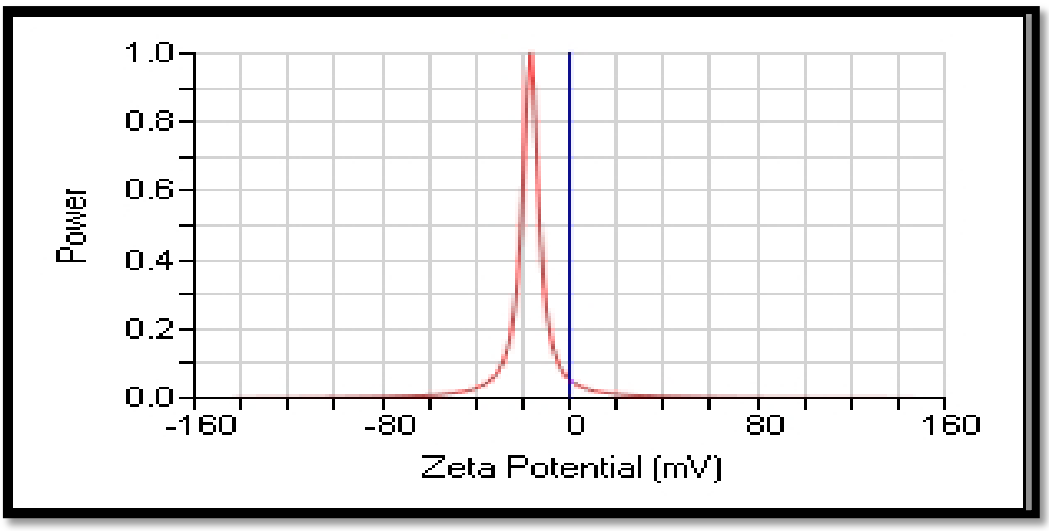

Figure 16-Zeta potential of CdO NPs.

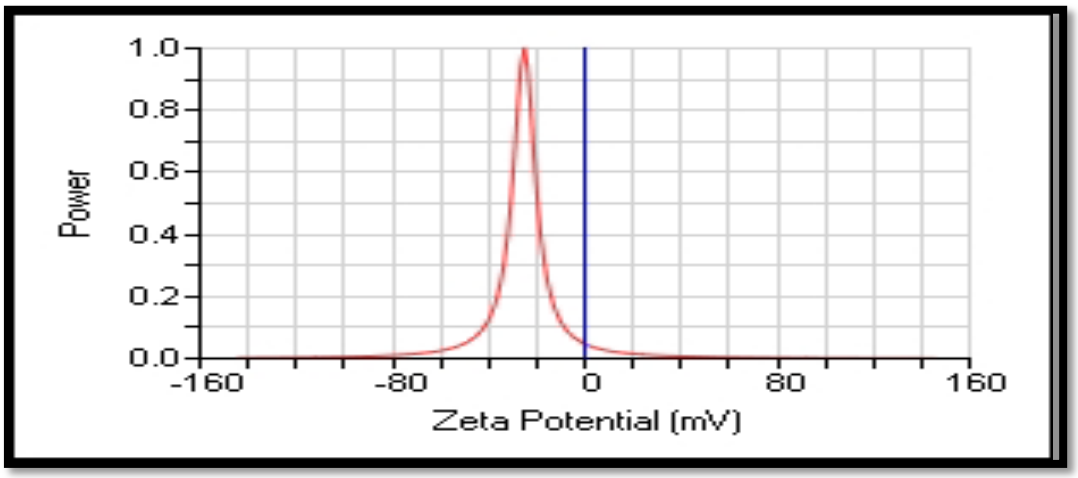

Figure 17-Zeta potential of Sn NPs.

Conclusions

In this work, colloidal metal NPs (Ag, Cu, ZnO, CdO, and Sn NPs) were successfully synthesized in de-ionized water by pulsed Nd: YAG laser ablation of pure metal targets. XRD results demonstrated the polycrystalline structure and the transformation from Zn and Cd to ZnO and CdO nanostructures. Absorbance data demonstrated an increase in the Plasmon peak with increasing laser power, indicating an increase in NP concentration. The zeta potential results showed that ZnO NPs are the most stabilized colloidal compared to other metals, while CdO NPs are the most aggregated colloidal**.**

References

1. Ramesh, K. T., Nanomaterials. In Nanomaterials (pp. 1-20). Springer, Boston, MA. **2009**.
2. Yin, Y., Rioux, R. M., Erdonmez, C. K., Hughes, S., Somorjai, G. A. and Alivisatos, A. P. **2004**. Formation of hollow nanocrystals through the nanoscale Kirkendall effect. *Science*, **304**(5671): 711-714.
3. Kong, X. Y., Ding, Y., Yang, R. and Wang, Z. L. **2004**. Single crystal nanorings formed by epitaxial self-coiling of polar nanobelts. *Science*, **303**(5662): 1348-1351.
4. Piriyawong, V., Thongpool, V., Asanithi, P. and Limsuwan, P. **2012**. Effect of laser pulse energy on the formation of alumina nanoparticles synthesized by laser ablation in water, *Procedia Engineering*, **32**: 1107-1112.
5. MIRELA, DRAGOMIR. **2009**. "Metallic Nanoparticles." University Of Nova Gorica (2009).
6. Kumar, H., Venkatesh, N., Bhowmik, H. and Kuila, A. **2018**. Metallic Nanoparticle: A Review. *Biomedical Journal of Scientific & Technical Research*, **4**(2): 3765-3775.

7. Mendivil, M. I. et al. **2014**. "Transmission electron microscopic studies on noble metal nanoparticles synthesized by pulsed laser ablation in liquid." Microscopy: *Advances in Scientific Research and Education*: 911-920.

8. Pearce, S. R. J., Henley, S. J., Claeyssens, F., May, P. W., Hallam, K. R., Smith, J. A. and Rosser, K. N., Production of nanocrystalline diamond by laser ablation at the solid/liquid interface. *Diamond and Related Materials*, **13**(4-8): 661-665, (2004).

9. Karthik, K., Selvan, G. K., Kanagaraj, M., Arumugam, S. and Jaya, N. V. **2011**. Particle size effect on the magnetic properties of NiO nanoparticles prepared by a precipitation method. *Journal of Alloys and compounds*, **509**(1): 181-184.

10. Yang, G. W. **2007**. Laser ablation in liquids: Applications in the synthesis of nanocrystals. *Progress in Materials Science*, **52**(4): 648-698.

11. Sasaki, T., Shimizu, Y. and Koshizaki, N. **2006**. Preparation of metal oxide-based nanomaterials using nanosecond pulsed laser ablation in liquids. *Journal of Photochemistry and Photobiology A: Chemistry*, **182**(3): 335-341.

12. Usui, H., Shimizu, Y., Sasaki, T. and Koshizaki, N. **2005**. Photoluminescence of ZnO nanoparticles prepared by laser ablation in different surfactant solutions. *The Journal of Physical Chemistry B*, **109**(1): 120-124.

13. Zeng, H., Li, Z., Cai, W., Cao, B., Liu, P. and Yang, S. **2007**. Microstructure control of Zn/ZnO core/shell nanoparticles and their temperature-dependent blue emissions. *The Journal of Physical Chemistry B*, **111**(51): 14311-14317.

14. Griffiths, D., Bernt, W., Hole, P., Smith, J., Malloy, A. and Carr, B. **2011**. Zeta Potential Measurement of Nanoparticles by Nanoparticle Tracking Analysis (NTA), In *NSTI-Nanotech*, **1**: 4-7.

15. Wang, P. and Keller, A. A. **2009**. Natural and engineered nano and colloidal transport: Role of zeta potential in prediction of particle deposition. *Langmuir*, **25**(12): 6856-6862.

16. Sun, D., Kang, S., Liu, C., Lu, Q., Cui, L. and Hu, B. **2016**. Effect of zeta potential and particle size on the stability of SiO2 nanospheres as carrier for ultrasound imaging contrast agents. *Int. J. Electrochem. Sci*, **11**(10): 8520-8529.

17. Habib, I. Y., Kumara, N. T. R. N., Lim, C. M. and Mahadi, A. H. **2018**. Dynamic Light Scattering and Zeta Potential Studies of Ceria Nanoparticles. In *Solid State Phenomena*, **278**: 112-120.

18. Imam, H., Elsayed, K., Ahmed, M. A. and Ramdan, R. **2012**. Effect of experimental parameters on the fabrication of gold nanoparticles via laser ablation. *Optics and Photonics Journal*, **2**(2).

19. Sanchez and D. Blazquez, **2007**. The Surface Plasmon Resonance of Supported Noble Metal Nanoparticles: Characterization, Laser Tailoring, and SERS Application. Madrid University, Madrid, Spain, (2007).